PHYSICAL REVIEW B **69**, 094416 (2004)

Ruthenium double perovskites: Transport and magnetic properties

R. I. Dass, J.-Q. Yan, and J. B. Goodenough
Texas Materials Institute, ETC 9.102, 1 University Station, C2201, University of Texas at Austin, Austin, Texas 78712-1063, USA

(Received 8 October 2003; published 17 March 2004)

The double perovskites $La_2MRuO_{6+\delta}$ contain M^{2+} ions for $M=$Mg, Zn, Co, and Ni and for $M=$Mn and Fe, M^{3+} ions. Annealed samples have ordered M^{2+} and Ru(IV), but samples with M^{3+} ions are atomically disordered and remain oxidized $(\delta>0)$ after annealing in a N_2 atmosphere. A comparison of quenched, air-annealed, and N_2-annealed $La_2MgRuO_{6+\delta}$ samples showed a persistence of a few cation vacancies in the presence of oxygen vacancies $(\delta<0)$. In quenched samples, oxygen vacancies are preferentially located between two Ru atoms, where they form a deep two-electron trap state, whereas the two-electron trap state formed at an oxygen vacancy between an M^{2+} and Ru(IV) is shallow. Magnetic as well as transport data indicate the π-bonding $4d$ electrons at the low-spin Ru atoms occupy itinerant-electron states of a π^* band even in the atomically ordered samples, but strong correlations introduce magnetic transitions among the π^* electrons. The $M=$Co and Ni samples exhibit a magnetic transition at some, if not all, of the π^* electrons on the Ru array below a T_{irr} independent of magnetic ordering on the M^{2+} ions, and below a $T_N\approx 26$ K$<T_{\mathrm{irr}}$, antiferromagnetic ordering of the M^{2+}-ion spins suppresses any spin on the intervening Ru(IV). The $M^{2+}:e^2$-O-Ru(IV)-O-$M^{2+}:e^2$ antiferromagnetic superexchange interaction is stronger than the ferromagnetic $M^{2+}:e^2$-O-Ru(IV)$:e^0$ interaction because of a weak intraatomic exchange with the π^*-electron spins on the Ru(IV) atoms. On the other hand, disordered $La_2MnRuO_{6.17(1)}$ is ferromagnetic with a magnetization at 5 K of $2.85\mu_B$ per formula unit (f.u.) in a magnetic field of 50 kOe. This finding is interpreted with a model in which the π-bonding orbitals on both the Mn and Ru are coupled to form a common ferromagnetic π^* band in which only the antibonding electrons are not spin paired. The strong next-nearest-neighbor interaction between Ru atoms made manifest in the ordered double perovskites provides an explanation of why the π^* bandwidth of the perovskite system $Sr_{1-x}Ca_xRuO_3$ may increase with x.

DOI: 10.1103/PhysRevB.69.094416 PACS number(s): 75.30.Cr, 72.80.Ga, 75.30.Et, 75.30.Kz

I. INTRODUCTION

The double perovskites La_2MRuO_6 ($M=$Mg, Mn, Ni, and Zn) were studied by Galasso and Darby[1] a number of years ago, but at that time no magnetic measurements were performed. Early work on the system $Sr_{1-x}Ca_xRuO_3$ led to the conclusion that the $4d$ electrons of these perovskites give an itinerant-electron ferromagnetism in $SrRuO_3$ with a Curie-Weiss susceptibility corresponding to a localized low-spin Ru(IV) moment, but the Weiss constant θ decreased smoothly with increasing x with a loss of long-range magnetic order where θ becomes negative[2,3] although $CaRuO_3$ was later shown[4] to retain ferromagnetic interactions. The $4d$ electrons of Ru(III) in $LaRuO_3$ are itinerant with no long-range magnetic order.[5] Battle *et al.*[6] studied double perovskites containing Ru(V) and found evidence of itinerant-electron magnetism as a result of Ru-O-O-Ru interactions.

In this paper the role of ruthenium in the double perovskites La_2MRuO_6 has been revisited; compounds with $M=$Mg or Zn are compared to those with $M=$Mn, Fe, Co, or Ni. This comparison allows a study of the $4d$ electrons at Ru(IV) in the absence of another transition-metal atom to provide insight into their behavior in the presence of a localized spin on a neighboring transition-metal atom. The comparison sheds light on why ordered La_2CoRuO_6 and La_2NiRuO_6 are antiferromagnetic in contrast to the ferromagnetism of ordered La_2CoMnO_6 (Ref. 7) and La_2NiMnO_6.[8] In addition, the varying energies of the M^{3+}/M^{2+} redox energies allow determination of the energy of the Ru(IV)/Ru(III) redox couple relative to these energies. Our observations show that the Ru atoms contribute a magnetic moment to the Curie-Weiss susceptibility at high temperatures; but below a magnetic transition, the itinerant-electron unpaired spin density appears to be small. Co^{2+} and Ni^{2+} magnetic moments couple antiparallel to one another across a Ru(IV) ion in ordered La_2CoRuO_6 and La_2NiRuO_6 whereas disordered La_2FeRuO_6 forms a spin glass, and disordered La_2MnRuO_6 is ferromagnetic. The varying roles of the π^* electrons are discussed and the ferromagnetism of $La_2MnRuO_{6.17(1)}$ and $LaSrMnRuO_{6.03(1)}$ is accounted for by an itinerant electron π^* band that includes both Mn and Ru t-orbital parentage. Finally, it is pointed out that the π-bonding next-near-neighbor Ru-O-O-Ru interactions in a perovskite are enhanced by a bending of the M-O-M bond angle from 180°, which explains why $CaRuO_3$ acts as if it had a broader π^* band than $SrRuO_3$.

II. EXPERIMENTAL PROCEDURES AND RESULTS

A. Synthesis

Compounds of the system $La_2MRuO_{6+\delta}$ were prepared both by the Pechini method[9] and by solid-state reaction. The water of crystallization of all precursor salts was determined by thermogravimetric analysis (TGA) with a heating rate of 1 °C/min in flowing air for lanthanum (III) nitrate, cobalt

(II) nitrate, magnesium (II) nitrate, and ruthenium (III) chloride, and in a flowing mixture of 5% H_2/Ar for iron (II) oxalate and nickel (II) nitrate. $La_2M RuO_{6+\delta}$ ($M=$Mg, Co, and Ni) samples were synthesized by the Pechini method with $La(NO_3)_3 \cdot 6.03(1)H_2O$, $Mg(NO_3)_2 \cdot 5.98(1)H_2O$, $Co(NO_3)_2 \cdot 5.94(1)H_2O$, $Ni(NO_3)_2 \cdot 5.99(1)H_2O$, and $RuCl_3 \cdot 3.00(1)H_2O$ as the starting materials. Stoichiometric quantities of the salts were first dissolved in deionized water and then 1.5 times the stoichiometric amount of citric acid was added to the stirring brown solutions to accomplish complete chelation. After 30 min of stirring, ethylene glycol was added to the brown chelated solutions, and these solutions were then heated to approximately 150 °C to allow the chelates to undergo polyesterification as well as to remove excess water. The volume of ethylene glycol was carefully adjusted to prevent the formation of Co, Ni, and/or Ru metal particles. The resulting black gels were completely dried in an oven, ground, and slowly decomposed in air at 400 °C for 24 h. The products, black powders, were ground, pressed into half-inch-diameter pellets 2 to 4 mm thick, and annealed in air at 800 °C for 12 h. All the samples annealed at 800 °C in air were then ground, re-pelletized, and annealed in 12 h intervals with subsequent regrinding and re-pelletizing in different flowing atmospheres at the temperatures and for the times indicated in Table I. Those annealed in N_2 were first kept at 800 °C for 12 h to prevent the formation of Ru metal particles. With the exception of the quenched samples, LMGR-Q1, LCOR-Q1, and LNIR-Q1, all samples were cooled to room temperature in their respective atmospheres at the cooling rates indicated in Table I; the quenched samples were obtained by rapidly plunging them into liquid N_2 after annealing in air for 9 h at 1150 °C.

Samples of $La_2M RuO_{6+\delta}$ ($M=$Mn, Fe, and Zn) and $LaSrMnRuO_{6+\delta}$ were prepared by solid-state reaction; powders of La_2O_3 precalcined in air at 1000 °C for 12 h, $SrCO_3$, $MnCO_3$, $FeC_2O_4.1.99(1)H_2O$, and RuO_2 dried at 150 °C for 24 h, were ground together in stoichiometric ratios. For $M=$Zn, 2% mol. excess of ZnO was added to compensate for Zn evaporation at higher temperatures. The mixed powders were then pressed into half-inch-diameter pellets 2 to 3 mm thick and annealed for 12 h at 600 °C in Ar or N_2 for $M=$Fe, at 800 °C in air for $M=$Zn, and at 800 °C in Ar or N_2 for $M=$Mn and $LaSrMnRuO_{6+\delta}$. The products were then ground, re-pelletized, and annealed in 6 to 12 h intervals with subsequent regrinding and re-pelletizing in different flowing atmospheres at the temperatures and for the times indicated in Table I. All samples were synthesized at $T \leqslant 1225$ °C to prevent Ru evaporation. The pellets of all samples were black and dense.

The oxygen stoichiometry, the $6+\delta$ of Table I, was determined by complete reduction in flowing 10% H_2/Ar to a mixture of La_2O_3, MgO ($M=$Mg), MnO ($M=$Mn), Fe ($M=$Fe), Co ($M=$Co), Ni ($M=$Ni), and Ru in a Perkin-Elmer Series 7 Thermogravimetric Analyzer (TGA) at a heating rate of 1 °C/min to 1035 °C. For $M=$Zn, a complete reduction to La_2O_3, Zn, and Ru in a flowing 10% H_2/Ar mixture initially took place; however, a 10 h isotherm at 1035 °C was deliberately implemented to ensure a complete evaporation of the low-melting Zn (melting point≈420 °C). The oxygen stoichiometry of all samples was reproducible.

The samples of nominal $La_2M RuO_6$ ($M=$Mg, Co, Ni, and Zn) annealed in air were oxygen stoichiometric for $M=$Mg and Co but exhibited oxygen hyperstoichiometry $\delta=0.10(1)$ for $M=$Ni (sample LNIR-A1) in agreement with Yoshii *et al.*[10] and $\delta=0.06(1)$ for $M=$Zn (sample LZNR-A1); all samples synthesized in flowing N_2 or quenched in liquid N_2 after annealing in air were oxygen deficient, the N_2-annealed samples having the largest concentration of oxygen vacancies. All nominal $La_2M RuO_{6+\delta}$ ($M=$Mn or Fe) samples remained oxygen hyperstoichiometric with $\delta \geqslant 0.12(2)$ despite firing in flowing Ar or N_2 with sample decomposition occurring at $T>1225$ °C in these atmospheres. A larger value of δ was obtained for slow-cooled, N_2-annealed LMNR-N1 [$\delta=0.38(2)$] versus the more rapidly cooled, Ar-annealed LMNR-R1 [$\delta=0.17(1)$] whereas Ar-annealed LFER-R1 with a $\delta=0.30(2)$ had a larger nonstoichiometry than the slower cooled N_2-annealed LFER-N1 [$\delta=0.12(2)$]. A small oxygen excess, $\delta=0.03(1)$, was also observed in Ar-annealed $LaSrMnRuO_{6+\delta}$.

B. Structure

The identification of all room-temperature phases and the determination of their lattice parameters were accomplished with a Philips PW 1729 powder x-ray diffractometer equipped with a pyrolytic graphite monochromator and Cu $K\alpha$ radiation ($\lambda=1.540\,59$ Å); KCl was the internal standard. Data were collected in steps of 0.020° over the range $10° \leqslant 2\theta \leqslant 110°$ with a count time of 15 s per step. Peak profiles were fitted with the program JADE and lattice parameters were refined by a least-square method developed by Novak and Colville.[11] The room-temperature lattice constants of the different samples are also given in Table I.

All samples of $La_2M RuO_{6+\delta}$ were single phase to x-ray diffraction; the diffractograms exhibited a series of superstructure reflections for $M=$Mg, Co, Ni, and Zn due to the ordering of the M and Ru atoms on the octahedral sites of the perovskite structure. These samples were highly crystalline with narrow powder x-ray diffraction peaks, Figs. 1(a) and 1(b); the structures were easily refined within the monoclinic space group $P2_1/n$ ($Z=2$) with a $\beta \approx 90°$ and the b-axis unique, which accommodated an ordering of M^{2+} and Ru(IV) ions into distinguishable $2c$ and $2d$ sites. An early neutron-diffraction study performed by Seinen *et al.*[12] on nominal La_2NiRuO_6 synthesized at 1400 °C in air also revealed ordering of the Ni^{2+} and Ru(IV) on the B sites and was best refined in the space group $P2_1/n$. A later study performed by Battle *et al.*[13] on a sample prepared in air at 1150 °C and slow cooled at 6 °C/h, on the other hand, suggested disordered Ni and Ru atoms on the octahedral sites of an orthorhombic *Pbnm* perovskite. Nominal La_2MgRuO_6 and La_2ZnRuO_6 were always found to be ordered in all previous studies.[14,15] No superstructure reflections, however, were observed for $M=$Mn and Fe or for $LaSrMnRuO_{6+\delta}$, Figs. 1(c) and 1(d), so that these samples with a random distribution of Mn/Fe and Ru over the octahedral sites of the perovskite structure could be easily refined within the ortho-

TABLE I. The synthesis conditions and room-temperature structural properties of $La_2MRuO_{6+\delta}$, $LaSrMnRuO_{6+\delta}$, $La_2CoMnO_{6-\delta}$, and $La_{2-x}\square_xNiMnO_{6+\delta}$ prepared under different conditions.

Sample	Synthesis conditions	Oxygen content, $6+\delta$	Space group	a (Å)	b (Å)	c (Å)	β (°)	$c/\sqrt{2a}$	V (Å^3)
$La_2MRuO_{6+\delta}$									
$M=Mg$									
LMGR-A1	1150 °C (36 h), air, cool 20 °C/h	6.00(2)	$P2_1/n$	5.606(1)	7.898(1)	5.592(1)	90.08(1)		247.59(12)
LMGR-N1	1100 °C (24 h), 1150 °C (36 h), N_2, cool 20 °C/h	5.84(2)	$P2_1/n$	5.604(1)	7.903(1)	5.588(1)	90.03(1)		247.48(12)
LMGR-Q1	LMGR-A1 at 1150 °C (9 h), air, quenched in liquid N_2	5.88(2)	$P2_1/n$	5.604(1)	7.900(1)	5.586(1)	90.08(1)		247.30(12)
$M=Mn$									
LMNR-R1	1100 °C (36 h), 1150 °C (24 h), Ar, cool 180 °C/h	6.17(1)	*Pbnm*	5.566(1)	5.648(1)	7.861(1)		0.9987(3)	247.12(12)
LMNR-N1	1100 °C (36 h), 1150 °C (60 h), N_2, cool 20 °C/h	6.38(2)	*Pbnm*	5.566(1)	5.606(1)	7.862(1)		0.9988(3)	245.32(12)
$M=Fe$									
LFER-R1	1100 °C (36 h), 1150 °C (24 h), Ar, cool 180 °C/h	6.30(2)	*Pbnm*	5.574(1)	5.610(1)	7.898(1)		1.0019(3)	246.97(12)
LFER-N1	1100 °C (36 h), 1150 °C (60 h), N_2, cool 20 °C/h	6.12(2)	*Pbnm*	5.572(1)	5.605(1)	7.895(1)		1.0019(3)	246.57(12)
$M=Co$									
LCOR-A1	1150 °C (36 h), air, cool 20 °C/h	6.00(1)	$P2_1/n$	5.650(1)	7.893(1)	5.574(1)	90.09(1)		248.58(12)
LCOR-N1	1100 °C (24 h), 1150 °C (36 h), N_2, cool 20 °C/h	5.86(2)	$P2_1/n$	5.664(1)	7.896(1)	5.578(1)	90.04(1)		249.46(12)
LCOR-Q1	LCOR-A1 at 1150 °C (9 h), air, quenched in liquid N_2	5.90(1)	$P2_1/n$	5.647(1)	7.886(1)	5.575(1)	90.11(1)		248.27(12)
$M=Ni$									
LNIR-A1	1150 °C (36 h), air, cool 20 °C/h	6.10(1)	$P2_1/n$	5.613(1)	7.883(1)	5.571(1)	90.04(1)		246.50(12)
LNIR-N1	1100 °C (24 h), 1150 °C (36 h), N_2, cool 20 °C/h	5.92(2)	$P2_1/n$	5.616(1)	7.886(1)	5.570(1)	90.05(1)		246.68(12)
LNIR-Q1	LNIR-A1 at 1150 °C (9 h), air, quenched in liquid N_2	5.96(1)	$P2_1/n$	5.617(1)	7.884(1)	5.579(1)	90.12(1)		247.06(12)
$M=Zn$									
LZNR-A1	1025 °C (138 h), air, cool 20 °C/h	6.06(1)	$P2_1/n$	5.684(1)	7.921(1)	5.594(1)	90.03(1)		251.86(12)
$LaSrMnRuO_{6+\delta}$									
LSMNR-R1	1225 °C (120 h), Ar, cool 180 °C/h	6.03(1)	*Pbnm*	5.566(1)	5.648(1)	7.838(1)		0.9957(3)	246.40(12)
$La_2CoMnO_{6-\delta}$[a]									
LCM-O3	1350 °C (12 h), O_2, cool 20 °C/h 600 °C (168 h), 3 atm O_2, furnace cooled	6.00(1)	$P2_1/n$	5.526(1)	7.775(1)	5.492(1)	90.01(1)		235.96(12)
LCM-Q1	1350 °C (16 h), air, cool 20 °C/h 1350 °C (3 h), air, quenched in liquid N_2	5.95(1)	$P2_1/n$	5.522(1)	7.764(1)	5.480(1)	90.01(1)		234.99(12)
$La_{2-x}\square_xNiMnO_{6+\delta}$[b]									
$x=0$									
LNM-R1	1350 °C (6 h), Ar, cool 180 °C/h	6.05(1)	$P2_1/n$	5.517(1)	7.748(1)	5.466(1)	90.01(1)		233.65(12)
$x=1/12$									
L2NM-O1	1350 °C (24 h), O_2, cool 20 °C/h	6.03(1)	$P2_1/n$	5.515(1)	7.742(1)	5.463(1)	90.05(1)		233.25(12)
$x=1/10$									
L1NM-O1	1350 °C (24 h), O_2, cool 20 °C/h	5.97(1)	$P2_1/n$	5.516(1)	7.742(1)	5.464(1)	90.04(1)		233.34(12)

[a] Reference 7.

[b] Reference 8.

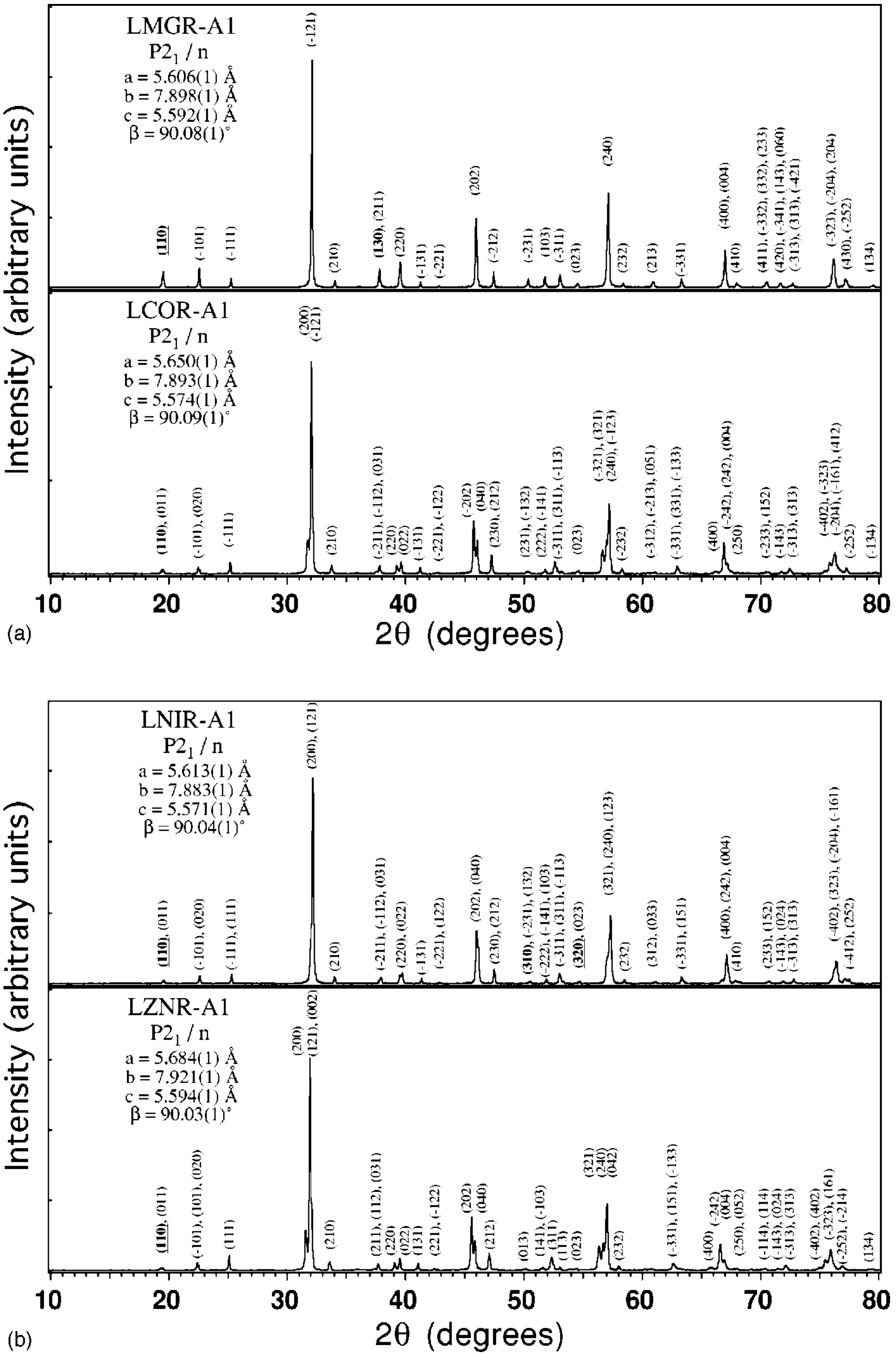

FIG. 1. The room-temperature powder x-ray diffraction patterns of some compositions in the systems $La_2M RuO_{6+\delta}$ and $LaSrMnRuO_{6+\delta}$. The $(hk0)$ reflections where h is an odd integer are underlined and shown in boldface type for samples of the monoclinic space group $P2_1/n$ (b-axis unique).

rhombic space group *Pbnm* $(Z=2)$. Nevertheless, a short-range ordering of the M and Ru atoms for $La_2M RuO_{6+\delta}$ ($M=$Mn or Fe) and $LaSrMnRuO_{6+\delta}$ can be expected as has been observed for nominal $LaSrMnRuO_6$.[16] A structural phase transition from orthorhombic *Pbnm* symmetry to rhombohedral $R\overline{3}c$ across a two-phase region in the temperature range 483 K$<T<$513 K has been observed for nominal $LaSrMnRuO_6$ with high-temperature x-ray diffraction; the transition has been verified to be first order with differential scanning calorimetry (DSC).[17] The presence of $(hk0)$ reflections in the powder x-ray diffractograms of all monoclinic $P2_1/n$ (b-axis unique) samples, where h is an odd integer, clearly distinguishes them from orthorhombic *Pbnm* samples in which all $(0kl)$ reflections, where k is also an odd integer, are systematically absent; the $(0kl)$ reflections in *Pbnm* are equivalent to the $(hk0)$ reflections in *Pnma*.

A $\delta>0$ is accommodated by the creation of cation vacancies since the perovskite structure cannot accept excess oxygen in an interstitial site. Tofield and Scott[18] and Mitchell *et al.*[19] have reported that these vacancies for $LaMnO_{3+\delta}$ and $La_{1-x}A_xMnO_{3+\delta}$ ($A=$alkaline earth) are preferentially on the La sites and have suggested that the extra extruded La is present as amorphous La_2O_3 that is undetected by a diffraction experiment. A recent study[8] on $Ln_{2-x}\square_xNiMnO_{6+\delta}$ (Ln=La or Nd) also reported for the monoclinic $P2_1/n$ phase an inhomogeneous preferential extrusion of the lan-

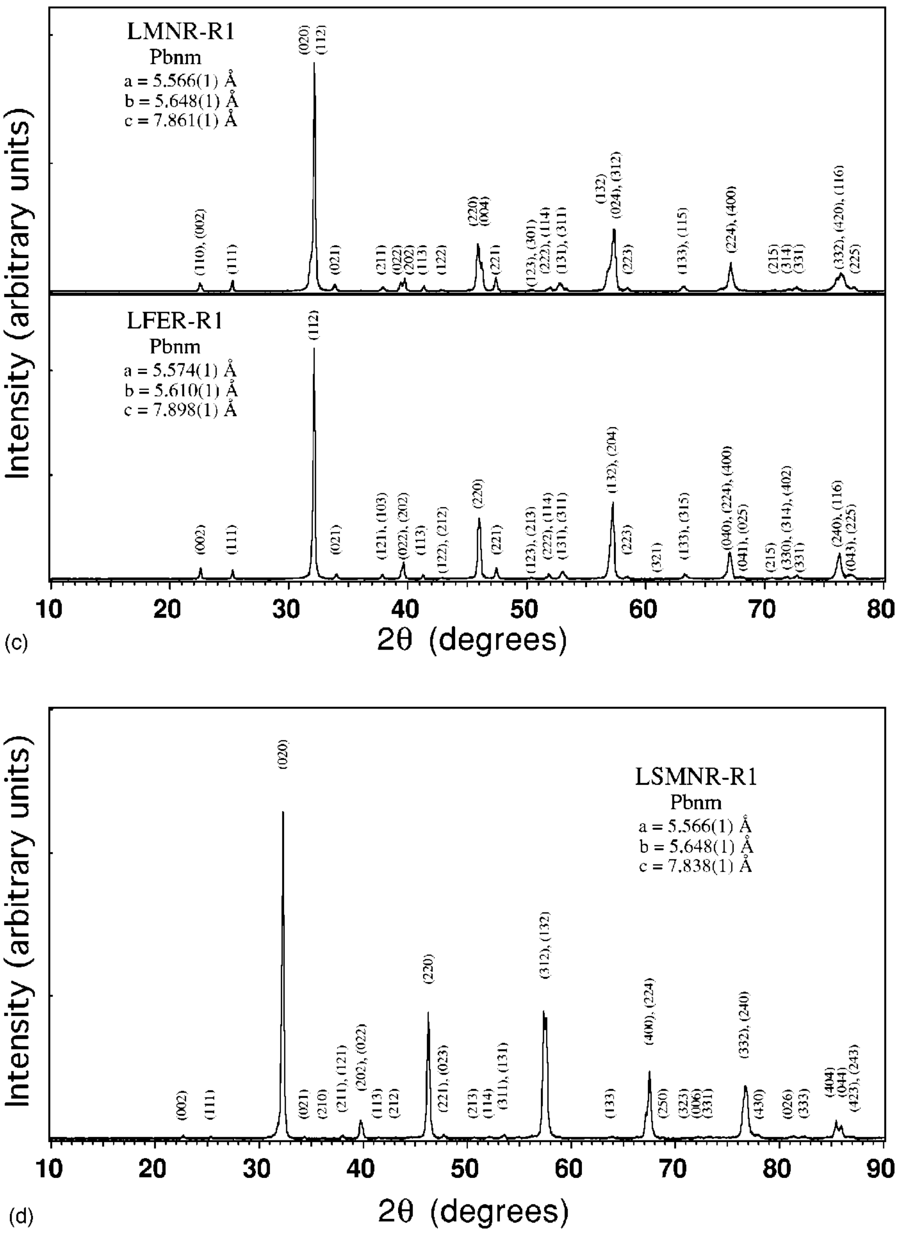

FIG. 1. (*Continued*).

thanide as Ln_2O_3 (Ln=La or Nd) and, therefore, a predominance of lanthanide vacancies over Ni and Mn vacancies.

Table I shows a nearly preparation-independent *a* parameter, cell volume *V*, and a $\beta \approx 90°$ for all samples indexed as monoclinic $P2_1/n$ for $La_2MgRuO_{6-\delta}$ and $La_2NiRuO_{6+\delta}$. For the monoclinic $P2_1/n$ $La_2CoRuO_{6-\delta}$ system, a $\beta \approx 90°$ was also observed, but a larger *a* parameter and volume *V* was found for the N_2-annealed sample, LCOR-N1, with the largest concentration of oxygen vacancies. A slightly larger volume for the more oxidized sample of orthorhombic $La_2FeRuO_{6+\delta}$, LFER-R1 [$\delta = 0.30(2)$] compared to LFER-N1 [$\delta = 0.12(2)$] is unusual. On the other hand, a smaller cell volume *V* for LMNR-N1 [$\delta = 0.38(2)$] compared to LMNR-R1 with $\delta = 0.17(1)$ is typical of a system with a more highly oxidized octahedral-site array.

C. Transport properties

The resistivity $\rho(T)$ of all samples was measured by a four-probe technique with a laboratory-built apparatus in the temperature range $5\,\mathrm{K} < T < 310\,\mathrm{K}$. The annealed, cold-pressed pellets of each sample were first cut into rectangular bars with average dimensions $0.5 \times 0.5 \times 3.5\,\mathrm{mm}^3$ and the four probes were mounted onto sputtered gold contacts on the sample surface using tiny In pads. All polycrystalline samples of $La_2MRuO_{6+\delta}$ and $LaSrMnRuO_{6+\delta}$, Fig. 2, were semiconductors with a low activation energy of conduction, E_σ, varying from 48 to 182 meV; the Mn-containing perovskites had the smallest values of $\rho(T)$ over all temperatures and the lowest activation energies, E_σ. The resistivities $\rho(T)$ of $La_2CoMnO_{6-\delta}$ and $La_{2-x}\square_x NiMnO_{6+\delta}$ (Ref. 8) were much greater than their Ru-containing analogues, $La_2CoRuO_{6-\delta}$ and $La_2NiRuO_{6+\delta}$.

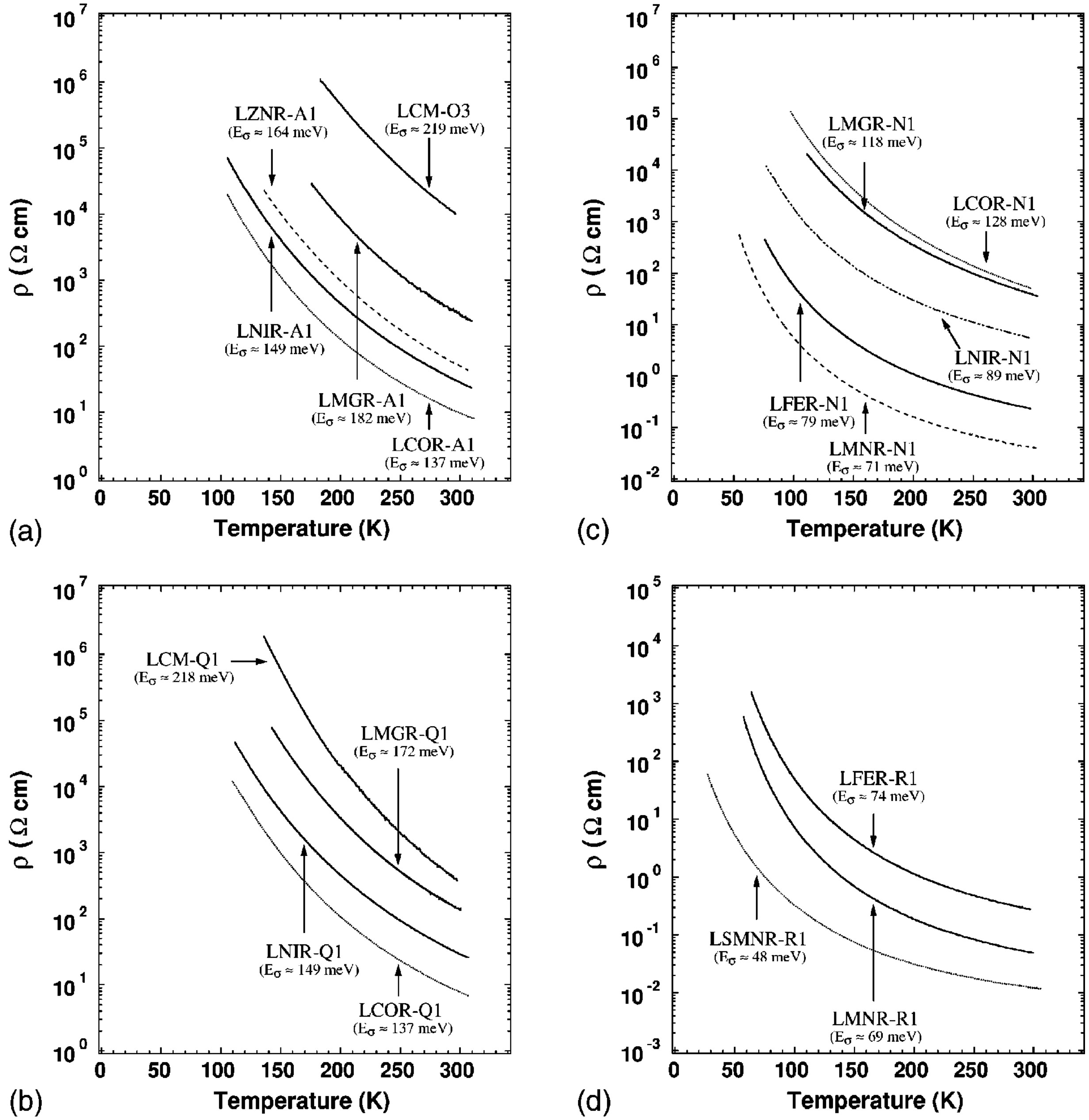

FIG. 2. The variation with temperature of the electrical resistivity $\rho(T)$ for compositions in the systems La_2MRu$O_{6+\delta}$ and LaSrMnRu$O_{6+\delta}$. The resistivities $\rho(T)$ of samples LCM-O3 and LCM-Q1 of $La_2CoMnO_{6-\delta}$ are also shown.

The Seebeck coefficient $\alpha(T)$ of all samples, Fig. 3, was obtained with a laboratory-built apparatus; a correction was applied to compensate for the small contribution to $\alpha(T)$ from the leads.

An activated behavior of the thermoelectric power with $E_a \approx 8$ meV was found in p-type LZNR-A1 for $T < 250$ K; a constant concentration of charge carriers was found above this temperature. An activated $\alpha(T)$ with $E_a \approx 7$ meV and 11 meV was also observed for p-type LFER-N1 and LFER-R1, respectively; a larger value of $\alpha(T)$ for the more oxidized LFER-R1 suggests a stronger trapping of holes in this material. The electronic properties of the samples are summarized in Table II.

D. Magnetic data

Magnetic data were taken with a Quantum Design dc superconducting quantum interference device (SQUID) magnetometer in the temperature range $5\ \mathrm{K} \leq T \leq 710$ K and in applied magnetic fields H from -50 kOe to 50 kOe. The M-H curves of all samples taken at 5 K are shown in Fig. 4. Before any measurements were made, the samples were heated to $T = 320$ K for La_2MRu$O_{6+\delta}$ and $T = 380$ K for LaSrMnRu$O_{6.03(1)}$ to remove any previous magnetic history.

Saturation of the magnetization was never attained in any of the samples of poorly ordered $La_2MnRuO_{6+\delta}$ and LaSrMnRu$O_{6.03(1)}$ for $H \leq 50$ kOe, Fig. 4(a). An $M(5\ \mathrm{K}, 50\ \mathrm{kOe}) \leq 2.85\mu_B$/f.u. for $La_2MnRuO_{6+\delta}$ and an

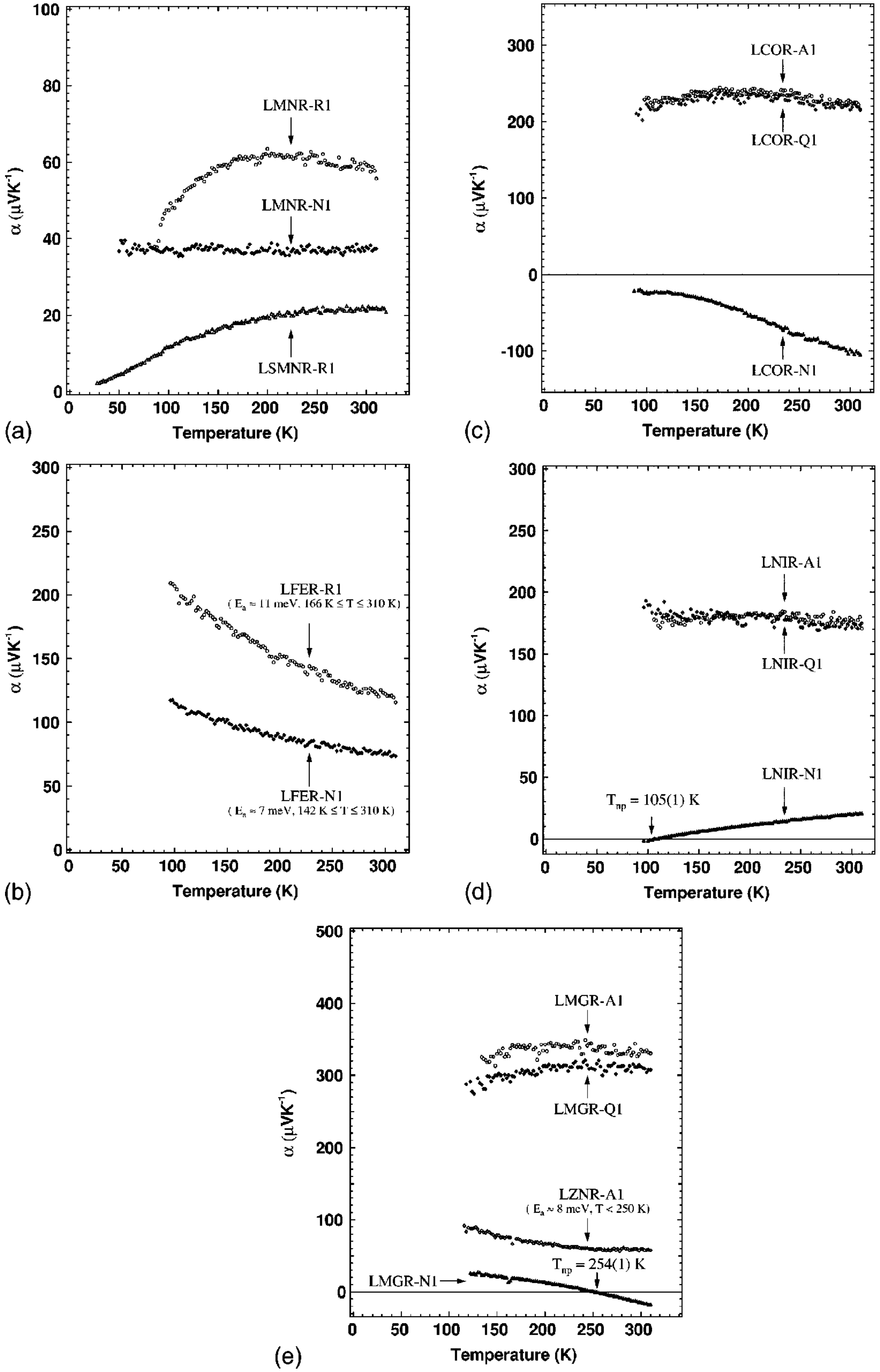

FIG. 3. The variation with temperature of the thermoelectric power $\alpha(T)$ for compositions in the systems $\mathrm{La_2}M\mathrm{RuO_{6+\delta}}$ and $\mathrm{LaSrMnRuO_{6+\delta}}$. The n-type to p-type transition temperature T_{np} is indicated for some of the compositions.

$M(5\ \mathrm{K},\ 50\ \mathrm{kOe}) = 2.30\mu_B/\mathrm{f.u.}$ for $\mathrm{LaSrMnRuO_{6.03(1)}}$ were observed. This observation is consistent with the low values of $M(5\ \mathrm{K},\ 50\ \mathrm{kOe}) = 2.0-3.2\mu_B/\mathrm{f.u.}$ and less than $3.1\mu_B/\mathrm{f.u.}$ previously reported for $\mathrm{La_2MnRuO_{6+\delta}}$ (Refs.

TABLE II. The electronic properties of $La_2MRuO_{6+\delta}$, $LaSrMnRuO_{6+\delta}$, $La_2CoMnO_{6-\delta}$, and $La_{2-x}\square_xNiMnO_{6+\delta}$ prepared under different conditions. E_σ, E_a, and ΔH_m are the activation energies of conduction, carrier generation, and carrier mobility, respectively. T_{np} is the n-type to p-type transition temperature from thermoelectric power measurements.

Sample	E_σ (meV)	E_a (meV)	ΔH_m (meV)	ρ(295 K) (Ω cm)	T_{np} (K)
$La_2MRuO_{6+\delta}$					
$M=Mg$					
LMGR-A1	182(8)			340	
LMGR-N1	118(5)			42	254(1)
LMGR-Q1	172(5)			150	
$M=Mn$					
LMNR-R1	69(2)			0.043	
LMNR-N1	71(2)	0	71(2)	0.051	
$M=Fe$					
LFER-R1	74(2)	11	63(2)	0.28	
LFER-N1	79(2)	7	72(2)	0.24	
$M=Co$					
LCOR-A1	137(5)			11	
LCOR-N1	128(5)			55	
LCOR-Q1	137(5)			8.5	
$M=Ni$					
LNIR-A1	149(5)			32	
LNIR-N1	89(3)			5.7	105(1)
LNIR-Q1	149(5)			32	
$M=Zn$					
LZNR-A1	164(6)	8 ($T<250$ K)	156(6) ($T<250$ K)	57	
		0 ($T>250$ K)	164(6) ($T>250$ K)		
$LaSrMnRuO_{6+\delta}$					
LSMNR-R1	48(2)	0 ($T>250$ K)	48(2) ($T>250$ K)	0.013	
$La_2CoMnO_{6-\delta}$					
LCM-O3	219(7)			10600	
LCM-Q1	218(5)			405	
$La_{2-x}\square_xNiMnO_{6+\delta}$[a]					
$x=0$					
LNM-R1	198(5)			395	
$x=1/12$					
L2NM-O1	238(6)			9100	316(2)
$x=1/10$					
L1NM-O1	237(5)			11400	

[a] Reference 8.

20–22) and nominal $LaSrMnRuO_6$,[23] respectively. Although the cations are disordered, the M-H hysteresis loops of these samples with an intrinsic coercivity $H_{ci}>3800$ Oe and a remanent magnetization $M_r\approx 1.3\mu_B$/f.u. are typical of a ferromagnet. On the other hand, the M-H hysteresis loops of the disordered $La_2FeRuO_{6+\delta}$ samples, Fig. 4(b), have a small remanent magnetization and 320 Oe$\leqslant H_{ci}\leqslant$480 Oe together with a clear shift of the M-H loops taken at $T=5$ K after field cooling (FC) in $H=2500$ Oe and 50 kOe from $T=320$ K, Fig. 4(c). Linear M-H curves with small coercivities $H_{ci}\leqslant 150$ Oe, Figs. 4(d) and 4(e), were found for antiferromagnetic $La_2CoRuO_{6-\delta}$ and $La_2NiRuO_{6+\delta}$. Samples of $La_2MgRuO_{6-\delta}$ also exhibited linear M-H behavior while a small deviation from linearity for applied fields with $|H|>12$ kOe and an M-H hysteresis with $H_{ci}=70$ Oe were observed in the M-H curve of $La_2ZnRuO_{6.06(1)}$, Fig. 4(f). The magnetic properties of the samples at 5 K are summarized in Table III.

Figure 5 shows the molar magnetization $M(T)$ and the molar magnetic susceptibility $\chi_{\mathrm{mol}}(T)$ for the samples of $La_2MRuO_{6+\delta}$ and $LaSrMnRuO_{6.03(1)}$ in different applied magnetic fields after cooling in zero field (ZFC) or cooling in the measuring field (FC). Before any measurements were made, the previous magnetic history was removed as de-

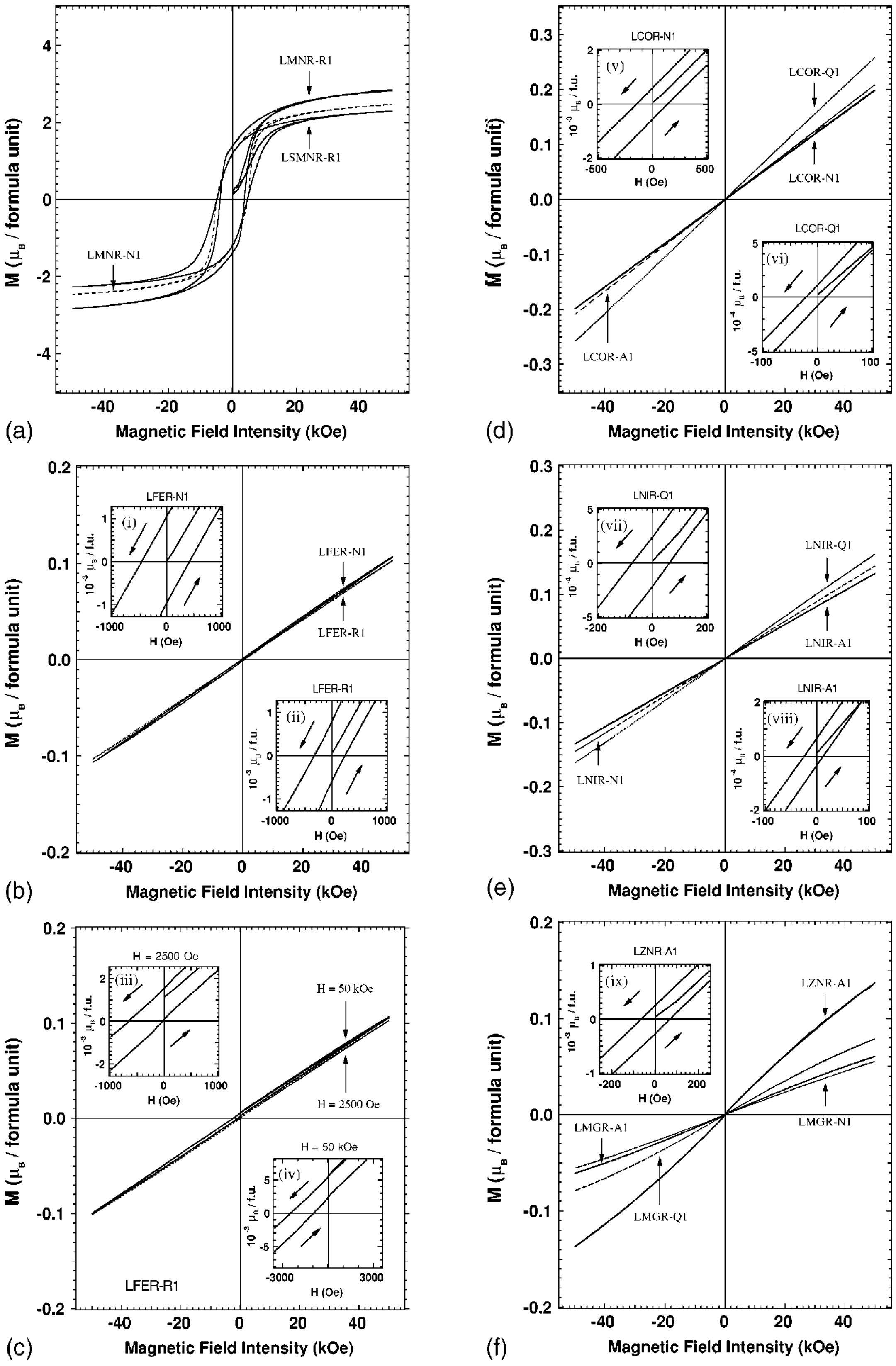

FIG. 4. The M-H hysteresis loops of some compositions in the systems $La_2MRuO_{6+\delta}$ and $LaSrMnRuO_{6+\delta}$ at $T=5$ K. Insets (i)–(ix) in (a)–(f) show the small coercivities and remanences for some of the compositions. A clear shift of the M-H loops for LFER-R1 taken at $T=5$ K after field cooling (FC) in $H=2500$ Oe and 50 kOe from $T=320$ K is shown in insets (iii) and (iv) in (c).

TABLE III. The magnetic properties of $La_2MRuO_{6+\delta}$ and $LaSrMnRuO_{6+\delta}$ prepared under different conditions. AF, F, SG, SP, and WF refer to antiferromagnetism, ferromagnetism, spin glass, superparamagnetic clusters, and weak ferromagnetism, respectively. T_{ci}, T_c^*, T_f, and T_N are the Curie temperature of long-range ferromagnetic order, the Curie temperature of ferromagnetic clusters, the spin-glass freezing temperature, and the Néel temperature of long-range antiferromagnetic order, respectively. $M(50\text{ kOe})$, M_r, and H_{ci} are the magnetization at 50 kOe, the remanent magnetization, and the coercivity, respectively. $\mu_{\text{eff,exp}}$ and $\mu_{\text{eff,calc}}$ are the experimental paramagnetic effective moment and the calculated, spin-only paramagnetic effective moment, respectively.

Sample	Type of magnetic behavior	Magnetic transition temperature (K)	$M(5\text{ K, }50\text{ kOe})$ $(\mu_B/\text{f.u.})$	M_r (5 K) $(\mu_B/\text{f.u.})$	H_{ci} (5 K) (Oe)	$\mu_{\text{eff,exp}}$ (μ_B)	$\mu_{\text{eff,calc}}$ (μ_B)	θ (K)
$La_2MRuO_{6+\delta}$								
$M=\text{Mg}$								
LMGR-A1	AF		0.061(1)	0	0	3.32(2)	2.83	$-134(2)$
LMGR-N1	AF		0.056(1)	0	0	3.43(2)	2.53	$-151(2)$
LMGR-Q1	AF		0.079(1)	0	0	3.54(4)	2.61	$-121(3)$
$M=\text{Mn}$								
LMNR-R1	F	$T_c=86(2)$	2.85(2)	1.38(2)	3850(10)	4.93(2)		108(2)
LMNR-N1	F	$T_{c2}=162(4)$	2.48(2)	1.17(2)	4880(10)	4.83(2)		104(2)
	F	$T_{c1}=76(2)$						
$M=\text{Fe}$								
LFER-R1	SG	$T_{f1}=32(1)$	0.10(1)	0.0008	330(5)	5.32(3)	6.40	$-408(12)$
LFER-N1	SG	$T_{f1}=24(4)$	0.11(1)	0.001	480(5)	5.55(3)	6.26	$-358(6)$
$M=\text{Co}$								
LCOR-A1	AF	$T_N=26(1)$	0.21(1)	7×10^{-5}	15(5)	5.65(2)	4.80	$-95(2)$
LCOR-N1	AF	$T_N=26(1)$	0.20(1)	0.0006	150(5)	5.62(2)	4.65	$-108(4)$
LCOR-Q1	AF	$T_N=26(1)$	0.26(1)	0.0001	20(5)	6.00(5)	4.69	$-98(2)$
$M=\text{Ni}$								
LNIR-A1	AF	$T_N=28(2)$	0.13(1)	7×10^{-5}	25(5)	4.28(2)	3.87	$-100(2)$
LNIR-N1	AF	$T_N=32(2)$	0.14(1)	0.0002	60(5)	4.63(5)	3.90	$-108(2)$
LNIR-Q1	AF	$T_N=26(2)$	0.16(1)	0.0002	80(5)	4.72(5)	3.95	$-104(4)$
$M=\text{Zn}$								
LZNR-A1	WF	$T_c=165(2)$	0.14(1)	0.0003	70(5)	3.40(2)	2.97	$-86(2)$
$LaSrMnRuO_{6+\delta}$								
LSMNR-R1	SP	$T_c^*=345(5)$	2.30(2)	1.19(2)	4810(10)	4.98(2)		204(2)
	F	$T_c=195(2)$						

scribed above. The magnetic transition temperatures T_c or T_c^* of Table III were taken from the inflection points of the low-field ($H=20$ Oe) data. The $M(T)$ and $M^{-1}(T)$ curves of $La_2MnRuO_{6+\delta}$ and $LaSrMnRuO_{6.03(1)}$, Figs. 5(a) and 5(b), clearly demonstrate ferromagnetic behavior; a single ferromagnetic phase with a $T_c=86(2)$ K and 195(2) K was found for LMNR-R1 and $LaSrMnRuO_{6.03(1)}$, respectively, whereas the $M(T)$ curve for sample LMNR-N1 $[\delta=0.38(2)]$ shows a majority ferromagnetic phase with $T_{c1}=76(2)$ K and a minority ferromagnetic phase with $T_{c2}=162(4)$ K. Considerable short-range magnetic order, however, was observed in $LaSrMnRuO_{6.03(1)}$ in the temperature range $T_c \leqslant T \leqslant T_c^*=345(5)$ K. A paramagnetic Weiss constant $\theta > T_c$ for LMNR-R1 and $LaSrMnRuO_{6.03(1)}$ and a $\theta > T_{c1}$ for LMNR-N1 are characteristic of ferromagnetic behavior as opposed to ferrimagnetism. This observation contrasts with the literature data. Spin-glass behavior below a $T_{\text{cusp}} \approx 45$ K and possible short-range ferrimagnetic/ferromagnetic order below 150 K have been reported[22] for a highly oxidized sample $La_2MnRuO_{6.39}$. Spin-glass behavior and Weiss constants $\theta=100$ and 120 K were also reported[20] for the compositions $\delta \approx -0.015$ and 0.152 of $La_2MnRuO_{6+\delta}$, respectively; however, an unusual enhancement in the FC data of $La_2MnRuO_{6.152}$ below 15 K was not explained. Both spin-glass behavior[23] and ferrimagnetism[16] below 250 K have also been reported for nominal samples of $LaSrMnRuO_6$.

A pronounced divergence between the ZFC and FC curves below a $T_{\text{irr}}=276(2)$ K and a sharp maximum in the ZFC and FC curves at a spin-glass freezing temperature $T_f=32(1)$ K were observed in the $H=100$ Oe $\chi_{\text{mol}}(T)$ data of LFER-R1 $[\delta=0.30(2)]$, Fig. 5(c); the application of an increasing applied magnetic field H greatly suppressed the maximum at T_f and obscured T_{irr}. A broad maximum at a $T_f=24(4)$ K, however, was found only in the ZFC curve of LFER-N1 while a pronounced divergence between the ZFC and FC curves below a $T_{\text{irr}}=365(5)$ K, similar to LFER-R1, and a nearly temperature independent $\chi_{\text{mol}}(T)$ for $125\text{ K} < T < 250\text{ K}$ in $H=100$ Oe, also Fig. 5(c), were both ob-

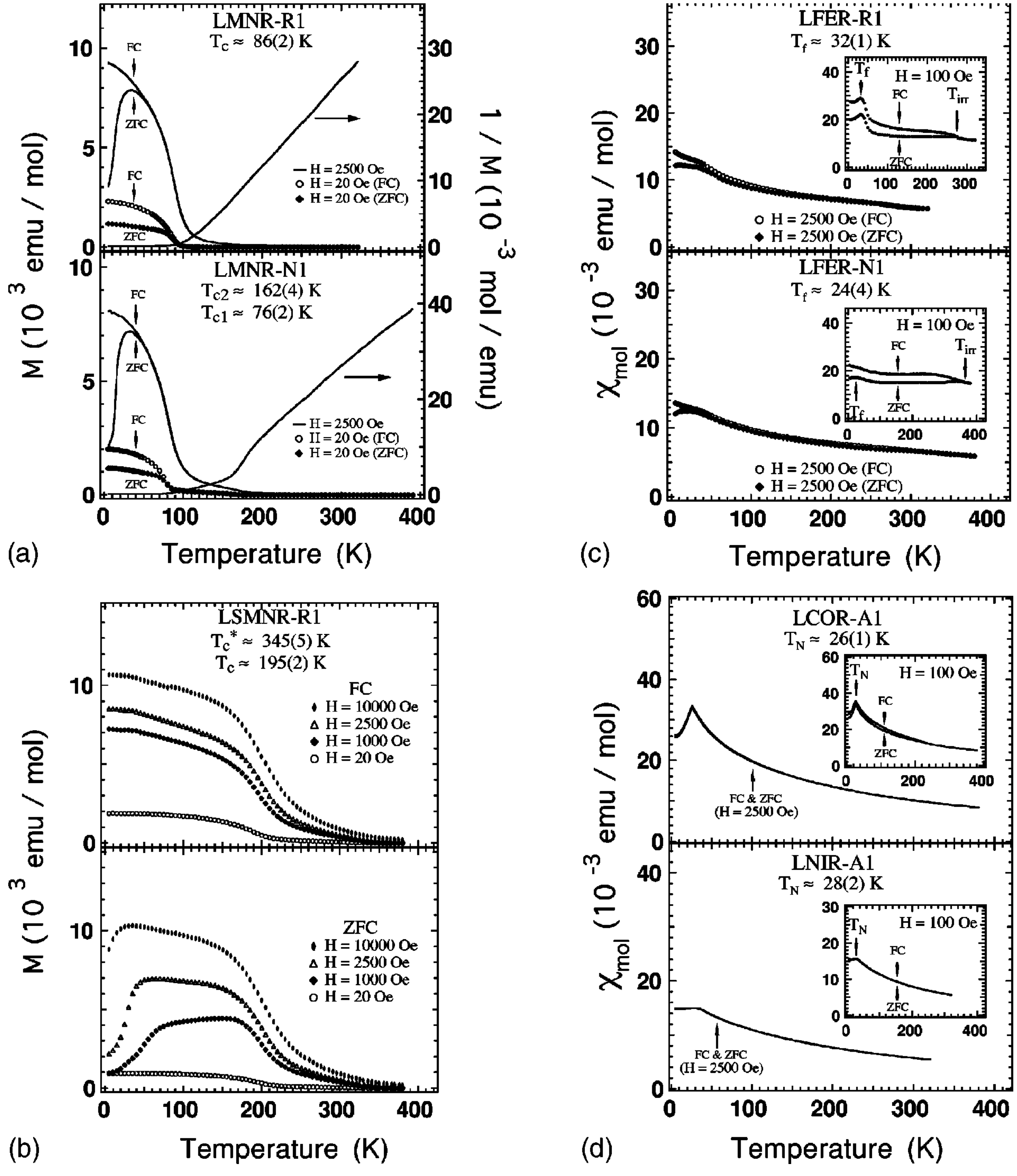

FIG. 5. The temperature dependence of the molar magnetization $M(T)$ and molar magnetic susceptibility $\chi_{\mathrm{mol}}(T)$ under different applied magnetic fields for some compositions in the systems $La_2MRuO_{6+\delta}$ and $LaSrMnRuO_{6+\delta}$.

scured by an increasing H. A large negative Weiss constant $\theta < -350$ K and a $\mu_{\mathrm{eff,exp}} < 5.92\mu_B$, the spin-only paramagnetic effective moment for high-spin Fe^{3+}, was found for all samples of $La_2FeRuO_{6+\delta}$.

All samples of $La_2CoRuO_{6-\delta}$ exhibited a sharp, well-defined cusp at a Néel temperature $T_N = 26(1)$ K, independent of δ and H, whereas less well-ordered samples of $La_2NiRuO_{6+\delta}$ had slightly broader cusps at similar Néel temperatures, $26(2)\ \mathrm{K} \leqslant T_N \leqslant 32(2)$ K, Figs. 5(d)–5(f). A $|\theta|/T_N \approx 4$ was found for all samples of $La_2CoRuO_{6-\delta}$ and $La_2NiRuO_{6+\delta}$. As in the $La_2FeRuO_{6+\delta}$ compounds, a small divergence of the FC and ZFC molar magnetic susceptibility was found below a $T_{\mathrm{irr}} \approx 230-270$ K. The $\chi_{\mathrm{mol}}^{-1}(T)$ plots of samples of $La_2MgRuO_{6-\delta}$, Figs. 5(g) and 5(h), showed a deviation from Curie-Weiss behavior below a $T_{\mathrm{CW}} \approx 265$ K that suggests antiferromagnetic ordering whereas a weak ferromagnetism was found below $T_{\mathrm{CW}} \approx 165$ K in $La_2ZnRuO_{6.06(1)}$.

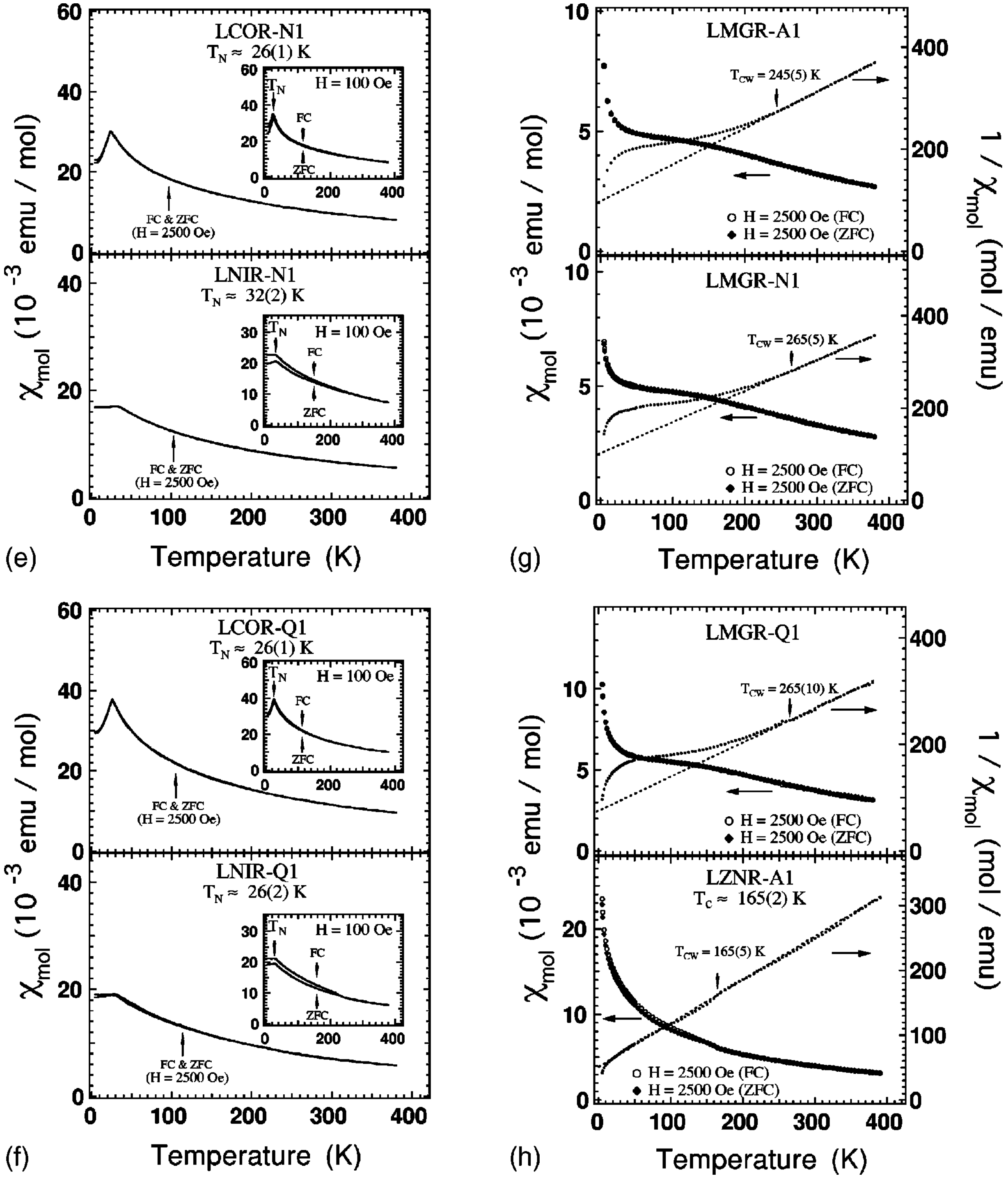

FIG. 5. (*Continued.*)

III. DISCUSSION

A. Placement of redox energies

The transport and magnetic properties of ordered La_2MgRuO_6 are consistent with a model in which the 4*d* electrons of the low-spin Ru(IV) ions occupy itinerant-electron states in a narrow π^* band of *t*-orbital parentage; but strong π^*-electron correlations separate the Ru(V)/Ru(IV) and Ru(IV)/Ru(III) redox couples by a small gap as indicated schematically in Fig. 6. This condition is possible because strong Ru-O covalent bonding lowers the intra-atomic Coulomb energy (the Hubbard *U*) and provides a substantial overlap of the 4*d* orbitals of next-nearest-neighbor Ru atoms. Moreover, the atomic ordering of La_2MRuO_6 for M=Co and Ni as well as for Mg and Zn signals the presence of Co^{2+} and Ni^{2+} in the presence of Ru(IV). Placement of the Co^{3+}/Co^{2+} and Ni^{3+}/Ni^{2+} redox energies below the Fermi energy ε_F means that oxidation and reduction takes place in the Ru(V)/Ru(IV) and Ru(IV)/Ru(III) couples, respectively. Consequently, the motional en-

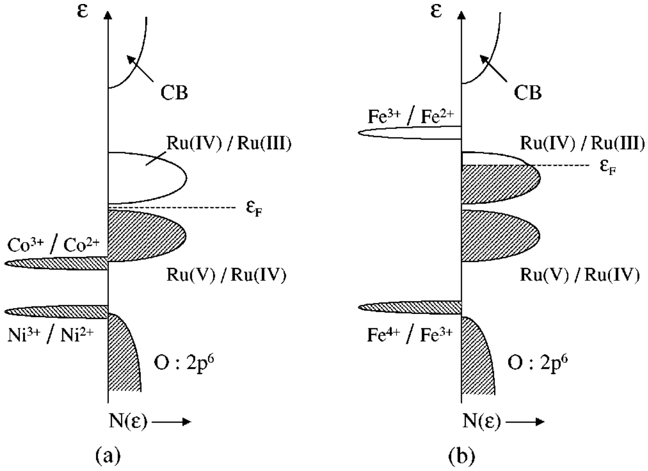

FIG. 6. Schematic of the relative positions of the redox energies in (a) nominal La_2CoRuO_6 and La_2NiRuO_6 and (b) $La_2FeRuO_{6+\delta}$ where CB is the conduction band.

thalpy $\Delta H_m = E_\sigma - E_a$ of the charge carriers of all the La_2MRuO_6 (M=Mg, Zn, Co, and Ni) are of similar small magnitude.

Bouchard *et al.*[24] have reported Mössbauer data showing the coexistence of Fe^{3+} and Ru(III) in $LaFe_{1-x}Ru_xO_3$, indicating that the Fe^{3+}/Fe^{2+} redox couple lies above the Ru(IV)/Ru(III) couple. The coexistence of Fe^{3+} and Ru(III) explains the lack of atomic order in $La_2FeRuO_{6+\delta}$ and the difficulty to reduce the compound to La_2FeRuO_6. With atomic disorder, nearest-neighbor as well as next-nearest-neighbor overlap of Ru $4d$ electrons occur, so the π^* polarons have a smaller motional enthalpy even though the octahedral-site array is disordered.

Although the Mn^{3+}/Mn^{2+} redox energy lies below the Fe^{3+}/Fe^{2+} redox energy, the manganese become Mn^{3+}. Therefore, $La_2MnRuO_{6+\delta}$ is also disordered and difficult to reduce to La_2MnRuO_6. Placement of the relative positions of the redox energies shown in Figs. 6 and 7 allows a qualitative interpretation of the thermoelectric power and magnetic data reported in Figs. 3 and 5. The lower resistivity $\rho(T)$ and motional enthalpy ΔH_m of $La_2MnRuO_{6+\delta}$ suggest that the electrons in half-filled t orbitals of the $Mn^{3+}:t^3e^1$ ions are converted to itinerant π^* electrons as a result of the strong overlap with the π^* electrons on the Ru ions. The thermoelectric power and magnetic data discussed below support this conclusion.

B. Thermoelectric power

The air-annealed $La_2MRuO_{6+\delta}$ (M=Mg, Zn, Co, and Ni) samples with $\delta \approx 0$ all have a large, positive nearly temperature-independent thermoelectric power $\alpha(T)$ characteristic of polaron conduction by a small concentration of mobile holes in the Ru(V)/Ru(IV) redox couple. Since interstitial oxygen is not incorporated into the perovskite structure, the holes must be introduced by cation vacancies. Surprisingly, the quenched samples with $\delta < 0$ also have a large, positive thermoelectric power; the electrons introduced by the oxygen vacancies are apparently trapped. On the other hand, lower or negative values of $\alpha(T)$ are encountered in the N_2-annealed samples with $\delta < 0$ where the M and Ru atoms are well ordered. From these observations, we draw the following conclusions: (1) the oxygen vacancies in the quenched samples, which have disordered M and Ru atoms, are preferentially located between two Ru atoms where electrons are trapped in a two-electron Ru(III)-□-Ru(III) bond across the vacancy; two-electron states from the Ru(IV)/Ru(III) couple are lowered to well below the Fermi energy ε_F as a result of a large overlap of Ru $4d$ wave functions at the oxygen vacancy; (2) in the well-ordered N_2-annealed samples where an oxygen vacancy is forced to lie between an M and a Ru atom, the $2+$ lattice charge at an oxygen vacancy traps one electron deeply at a primarily Ru(III) trap state, but the second electron in this trap is at a Ru(III) that does not border the vacancy, which raises the two-electron trap energy to just below ε_F; (3) the persistence of an $\alpha(T) > 0$ in the quenched samples means a small concentration of cation vacancies is present even in samples with $\delta < 0$. Since a competitive hole concentration is found in all the $La_2MRuO_{6+\delta}$ samples with $\delta < 0$, we conclude that some cation vacancies are an intrinsic property of all samples; we suspect a small concentration of La^{3+} is lost as amorphous La_2O_3.

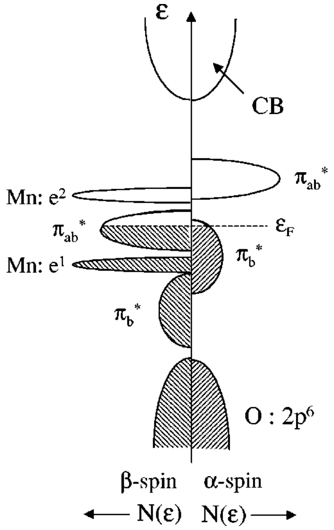

FIG. 7. Schematic of the relative positions of the redox energies for ferromagnetic $La_2MnRuO_{6+\delta}$ where CB is the conduction band; π_b^* and π_{ab}^* refer to bonding and antibonding bands with respect to the metal-metal interactions.

The N_2-annealed sample $La_2MgRuO_{5.84(2)}$ appears to be well ordered, and a progressive trapping out of the second electron at the oxygen vacancies on lowering the temperature converts an $\alpha(T) < 0$ to an $\alpha(T) > 0$ because of the presence of a competitive hole concentration from cation vacancies having a smaller trapping energy.

In the case of $La_2ZnRuO_{6.06(1)}$, a $\delta > 0$ introduces a greater concentration of cation vacancies. Since not all the holes introduced by a cation vacancy are trapped, a larger hole concentration than that in nominal $La_2MgRuO_{6.00(2)}$ lowers the nearly temperature independent $\alpha(T)$ to about 60

$\mu V K^{-1}$ above 250 K, but the onset of a rise in $\alpha(T)$ on cooling below 250 K signals an additional trapping of holes at the lower temperatures.

The $\alpha(T)$ curves for the N_2-annealed $La_2CoRuO_{5.86(2)}$ and $La_2NiRuO_{5.92(2)}$ samples both show the coexistence of hole and electron charge carriers; but the larger oxygen-vacancy concentration in the former makes $\alpha(300\,K)<0$ whereas the latter has $\alpha(300\,K)>0$. Although the polycrystalline $\rho(T)$ data had a semiconductive temperature dependence, the $\alpha(T)$ curves approach the linear temperature dependence with a low-temperature phonon-drag anomaly predicted for itinerant electrons; hole and electron trapping, however, do not fully determine the $\alpha(T)$ behavior of these two compounds.

All the disordered $La_2FeRuO_{6+\delta}$ samples contain cation vacancies and no, or few, oxygen vacancies. Therefore, these perovskites are p-type and show a progressive trapping out of mobile holes, which raises $\alpha(T)$ with decreasing temperature.

Our interpretation of the transport and magnetic properties of the disordered and ferromagnetic $La_2MnRuO_{6.17(1)}$ and $LaSrMnRuO_{6.03(1)}$ is based on a model in which the π^* band of t-orbital parentage includes the π-bonding electrons of the Mn^{3+} ions. In this model, the π^* band would contain 7.66 electrons/f.u. for $La_2MnRuO_{6.17(1)}$. An itinerant-electron ferromagnetic band normally has spin-paired bonding electrons; the ferromagnetic moment comes primarily from the antibonding electrons as is illustrated by the Slater-Pauling curves for the ferromagnetic $3d$ transition metals and their alloys.[25] Here we refer to π^*-band bonding and antibonding states with respect to the metal-metal, not the metal-oxygen interactions. Therefore, a ferromagnetic π^* band in $La_2MnRuO_{6.17(1)}$ would place 1.66 electrons/f.u. in a majority-spin antibonding band containing 3.0 states/f.u., which makes it more than half-filled, see Fig. 7. Moreover, any transfer of electrons from the minority-spin bonding band to the majority-spin antibonding band would make both bands hole conductors to give an $\alpha(T)>0$. On the other hand, $LaSrMnRuO_{6.03(1)}$ would have only 0.94 electrons/f.u. in the majority-spin antibonding band so some transferred electrons from the minority-spin bonding bands to the antibonding bands is required to give an $\alpha(T)>0$ according to the model of Fig. 7. Well below the ferromagnetic Curie temperature T_c, $\alpha(T)$ for $LaSrMnRuO_{6.03(1)}$ increases linearly with temperature as predicted for itinerant holes, but above T_c a temperature independent $\alpha(T)$ is characteristic of vibronic or polaronic conduction; spin-disorder scattering could be responsible for a transition from itinerant to vibronic conduction.

The large cation-vacancy concentration in $La_2MnRuO_{6.38(2)}$ would leave the majority-spin antibonding band less than half-filled. However, the magnetic data reveal that a chemical inhomogeneity has been introduced; a ferromagnetic phase with a high T_c coexists with the phase having the Mn-Ru π^* band. A Mn-rich phase with fluctuating occupied e orbitals on Mn^{3+} ions would provide ferromagnetic vibronic-superexchange interactions between high-spin $Mn^{3+}{:}t^3e^1$ ions[26–28] and such a coupling would give a high T_c. A Mn-rich second phase would leave a Ru-rich disordered phase with an antibonding majority-spin π^* band more than half-filled. A temperature independent $\alpha(T)$ to low temperatures means that the mobile polaronic holes are not trapped at the lowest temperatures of our measurements.

C. Magnetism

The $La_2MgRuO_{6-\delta}$ samples all have a Curie-Weiss paramagnetic susceptibility above T_{CW}, but the molar Curie constant gives a μ_{eff} larger than that calculated for a spin-only $(S=1)$ localized electron $Ru(IV){:}t^4e^0$ configuration; the $4d$ electrons apparently occupy the itinerant-electron states of a π^* band of t-orbital parentage even where atomic order allows interactions only between next-nearest-neighbor octahedral-site cations. With a π^* band two-thirds filled as in ferromagnetic $SrRuO_3$, we can expect ferromagnetic correlations with a net moment per Ru atom between 1 and $2\mu_B$; the correlations appear to remain ferromagnetic in $CaRuO_3$ even though its Weiss constant θ is negative[4] as in $La_2MgRuO_{6.00(2)}$. Therefore, we believe the deviation of $\chi_{mol}(T)$ from the Curie-Weiss law below T_{CW} reflects the onset of a helical spin-density wave rather than short-range, frustrated antiferromagnetic fluctuations. The M-H curves at 5 K of Fig. 4(f) show no remanence in accord with antiferromagnetic order. The quenched sample has a higher value of $\chi_{mol}(T)$ than that of the ordered samples and a slight bending of the M-H curve toward the H axis at higher magnetic field strengths. This behavior is even more pronounced in the M-H curve for the $La_2ZnRuO_{6.06(1)}$ sample, a sample that exhibits a weak ferromagnetic component below a $T_{CW}\approx 165$ K and a small remanence in the M-H curve at 5 K. The weak ferromagnetism may be associated with cation vacancies that trap holes on the neighboring Ru atoms.

An original motivation for studying the double perovskites La_2MRuO_6 was to determine whether the $M^{2+}{:}e^2$-O-$Ru(IV){:}t^4e^0$ interactions would be ferromagnetic as found for $M^{2+}{:}e^2$-O-$Mn(IV){:}t^3e^0$ interactions in ordered La_2CoMnO_6 (Ref. 7) and La_2NiMnO_6.[8] The finding that ordered La_2CoRuO_6 and La_2NiRuO_6 are antiferromagnetic below a $T_N\approx 26$ to 32 K and exhibit a difference in their FC and ZFC $\chi_{mol}(T)$ curves below a $T_{irr}>T_N$, Figs. 5(d)–5(f) is quite remarkable. Since the magnetic ordering within the π^* band of the Ru subarray sets in below a $T_{CW}\approx 265$ K in La_2MgRuO_6, a temperature comparable to T_{irr}, we conclude that a magnetic ordering among at least some π^* electrons of the Ru subarray occurs below T_{irr} independently of ordering of the σ-bonding e electrons and that below T_N the antiferromagnetic $M^{2+}{:}e^2$-O-Ru(IV)-O-$M^{2+}{:}e^2$ interactions dominate any ferromagnetic $M^{2+}{:}e^2$-O-$Ru(IV){:}\pi^{*4}e^0$ interactions. The itinerant character of the π^* electrons does not provide a sufficiently large intraatomic exchange energy on the Ru(IV) to stabilize a competitive ferromagnetic $M^{2+}{:}e^2$-O-$Ru(IV){:}\pi^{*4}e^0$ interaction. An antiferromagnetic coupling across the σ-bond molecular orbital of a $Ru(IV)O_{6/2}$ cluster would annihilate any weak spin polarization of the Ru(IV) ions and give an antiferromagnetic order of the M^{2+} ions like that found in MnO.

The disordered $La_2FeRuO_{6+\delta}$ samples also have a T_{irr} below which the magnetic susceptibility behaves as if it contained ferromagnetic or superparamagnetic clusters in the range $T_f<T<T_{irr}$; these clusters are presumably Ru-rich regions about a cation vacancy. Below T_f, the spins of the disordered Fe^{3+} ions freeze in a spin-glass state as a result of frustrated antiferromagnetic interactions between the Fe^{3+}:t^3e^2 configurations. Moreover, a measured μ_{eff} smaller than that for just the Fe^{3+} contribution may reflect antiferromagnetic nearest-neighbor Fe^{3+} pairs in the temperature range of our measurements. Although these two types of short-range order occur independently of the spin-glass formation below T_f, displacement of the M-H hysteresis in FC measurements, Fig. 4(c), signals the existence of ferromagnetic clusters exchange coupled to an antiferromagnetic matrix.[29]

The single magnetic transition in the disordered, ferromagnetic $La_2MnRuO_{6.17(1)}$ sample shows that, in this compound, the magnetic coupling of the itinerant π^* spins and the e-electron spins are not decoupled, which led us to the model of Fig. 7. According to the model, the Mn:e^1-O-Ru(IV)-O-Mn:e^1 and Mn:e^1-O-Mn:e^1 interactions would be ferromagnetic by vibronic superexchange as in $LaMn_{1-x}Ga_xO_3$ (Refs. 26–28) and the Mn-Ru π^* bands would give a net ferromagnetic moment of $1.66\mu_B$/f.u. if only the antibonding electrons are magnetized in zero applied magnetic field. The predicted spin-only saturation magnetization at 0 K would then be $2.66\mu_B$/f.u., which is to be compared with a measured magnetization of $2.85\mu_B$/f.u. at 5 K in 50 kOe. The larger measured value compared to that predicted in zero applied magnetic field is the result of some electron transfer from the minority-spin to the majority-spin band induced by $H=50$ kOe. A comparable increase in M by an applied $H=50$ kOe has also been noted for $SrRuO_3$. On the other hand, the discrepancy may also be due to an increased magnetization of the π^* electrons in the vicinity of the cation vacancies. According to the model, $LaSrMnRuO_{6.03(1)}$ would have only 0.94 antibonding π^* electrons per formula unit if there were no transfer of electrons from the minority-spin band, so the ferromagnetic magnetization should be reduced by about $0.72\mu_B$/f.u. relative to that of $La_2MnRuO_{6.17(1)}$. An observed reduction of only $0.36\mu_B$/f.u. at $H=50$ kOe is in satisfactory agreement in view of the need for electron transfer from the minority-spin band to obtain a positive thermoelectric power and uncertainties in the role of the cation vacancies. From Fig. 7 it is apparent that there would be a larger transfer of minority-spin electrons in the case of $LaSrMnRuO_{6.03(1)}$.

D. Final comment

In our discussion we have referred to the perovskite system $Sr_{1-x}Ca_xRuO_3$, which exhibits a Curie-Weiss paramagnetic susceptibility with a Weiss constant θ and ferromagnetic Curie temperature T_c that decrease progressively with increasing x, the ferromagnetism disappearing where θ becomes negative apparently without loss of ferromagnetic correlations among the π^* electrons of the low-spin Ru(IV) array. Substitution of Ca for Sr in $Sr_{1-x}Ca_xMnO_3$ lowers the Néel temperature T_N because of a weakening t^3-O-t^3 antiferromagnetic interaction. Since this interaction has been thought to be solely due to a superexchange coupling between half-filled t orbitals, it has been generally assumed that an increased bending of the Mn-O-Mn bond and/or a stronger inductive effect on substitution of a more acidic Ca^{2+} ion for Sr^{2+} is responsible for lowering T_N. However, it has recently been shown[30] that the lowering of T_N with increased bending of the Mn-O-Mn bond is due primarily to the dominant σ-bond semicovalent-exchange component of the interactions. Therefore, the widespread assumption that the π^* band of $Sr_{1-x}Ca_xRuO_3$ is being progressively narrowed as x increases has no firm foundation. In view of the strong next-nearest-neighbor interactions of the Ru subarray in the La_2MRuO_6 double perovskites that are revealed in this study, the role of the next-nearest-neighbor interactions on the width of the π^* band of $Sr_{1-x}Ca_xRuO_3$ must be considered, and the strength of these interactions increases with bending of the Ru-O-Ru bond.[31] Therefore, one can interpret the evolution of magnetic properties in $Sr_{1-x}Ca_xRuO_3$ as a manifestation of the disappearance of long-range ferromagnetic order because the π^* band broadens with increasing x, long-range order vanishing before the magnetic susceptibility loses its Curie-Weiss temperature dependence. Strong correlation fluctuations in the paramagnetic state preserve the Curie-Weiss paramagnetism, but with a Weiss constant θ that becomes progressively more negative as the width of the π^* band increases.

IV. CONCLUSIONS

A systematic investigation of the double perovskites $La_2MRuO_{6+\delta}$ has led to the following findings and deductions:

(1) The M atom is present as M^{2+} for $M=$Mg, Zn, Co, and Ni; it is present as M^{3+} ions for $M=$Mn or Fe.

(2) An M^{2+}/Ru(IV) pair can be ordered by annealing at 1100 °C to 1150 °C and slow cooling whereas M^{3+} ions do not order.

(3) An oxygen vacancy creates a two-electron trap state; the trap state is deep where the vacancy is between two Ru atoms and is shallow where it is between an M and a Ru atom.

(4) Although the low-spin Ru(IV) ions of ordered La_2MRuO_6 compositions have only next-nearest-neighbor Ru-Ru interactions, nevertheless the Ru $4d$ electrons form itinerant-electron π^* bands of t-orbital parentage; but strong correlations among the π^* electrons introduce a finite energy gap between the Ru(V)/Ru(IV) and Ru(IV)/Ru(III) redox bands and a Curie-Weiss paramagnetic susceptibility.

(5) Cation vacancies trap higher valence states at neighboring cations, but they also contribute mobile holes to the Ru(V)/Ru(IV) redox band.

(6) Ordered La_2CoRuO_6 and La_2NiRuO_6 exhibit two magnetic transitions: an ordering of at least some Ru π^*-electron spins is found in an interval $T_N<T<T_{irr}$, but below $T_N\approx 26$ K, the M^{2+}-ion spins couple antiferromagnetically across a $RuO_{6/2}$ complex. Lack of ferromagnetic

coupling between the Co^{2+} or Ni^{2+} and Ru(IV) ions in these ordered double perovskites is attributed to the strong Ru $4d$, O $2p$ covalent mixing, which makes the intraatomic spin-spin coupling among the π^* electrons or between an e electron transferred to a Ru(IV) and a π^*-electron spin density weaker than the e-electron M-O-Ru-O-M superexchange interaction. However, a ferromagnetic M^{2+}:e^2-O-Ru:t^4e^0 interaction might be manifest in a ruthenium perovskite with a more dilute concentration of M^{2+} ions.

(7) The disordered $La_2FeRuO_{6+\delta}$ perovskite forms a spin-glass consisting of ferromagnetic regions coupled to an antiferromagnetic matrix.

(8) The transport and magnetic properties of the disordered, ferromagnetic $La_2MnRuO_{6.17(1)}$ and $LaSrMnRuO_{6.03(1)}$ perovskites can be interpreted with a model of ferromagnetic, itinerant π^* bands of t-orbital parentage from both Mn and Ru atoms.

(9) The observation of strong next-nearest-neighbor interactions between Ru(IV) ions provides an explanation of why the width of the π^* band of the system $Sr_{1-x}Ca_xRuO_3$ may increase with x.

ACKNOWLEDGMENTS

The authors are grateful to the National Science Foundation and the Robert A. Welch Foundation of Houston, TX, for financial support.

---

[1] F. Galasso and W. Darby, Inorg. Chem. **4**, 71 (1965).

[2] A. Callaghan, C.W. Moeller, and R. Ward, Inorg. Chem. **5**, 1572 (1966).

[3] J.M. Longo, P.M. Raccah, and J.B. Goodenough, J. Appl. Phys. **39**, 1327 (1968); J.B. Goodenough and J.M. Longo, in *Landolt-Börnstein Tabellen*, edited by K.-H. Hellwege (Springer-Verlag, Berlin, 1970), New Series, Group III, Vol. 4(a), p. 224.

[4] K. Yoshimura, T. Imai, T. Kiyama, K.R. Thurber, A.W. Hunt, and K. Kosuge, Phys. Rev. Lett. **83**, 4397 (1999).

[5] R.J. Bouchard and J.F. Weiher, J. Solid State Chem. **4**, 80 (1972).

[6] P.D. Battle, J.B. Goodenough, and R. Price, J. Solid State Chem. **46**, 234 (1983).

[7] R.I. Dass and J.B. Goodenough, Phys. Rev. B **67**, 014401 (2003).

[8] R.I. Dass, J.-Q. Yan, and J.B. Goodenough, Phys. Rev. B **68**, 064415 (2003).

[9] M. Pechini, U.S. Patent No. 3,330,697 (1967).

[10] K. Yoshii, H. Abe, M. Mizumaki, H. Tanida, and N. Kawamura, J. Alloys Compd. **348**, 236 (2003).

[11] G.A. Novak and A.A. Colville, Am. Mineral. **74**, 488 (1989).

[12] P.A. Seinen, F.P.F. van Berkel, W.A. Groen, and D.J.W. Ijdo, Mater. Res. Bull. **22**, 535 (1987).

[13] P.D. Battle and C.W. Jones, Mater. Res. Bull. **22**, 1623 (1987).

[14] P.D. Battle, J.R. Frost, and S.-H. Kim, J. Mater. Chem. **5**, 1003 (1995).

[15] J.-H. Choy, J.-Y. Kim, S.-H. Hwang, S.-J. Kim, and G. Demazeau, Int. J. Inorg. Mater. **2**, 61 (2000).

[16] K. Ramesha, V. Thangadurai, D. Sutar, S.V. Subramanyam, G.N. Subanna, and J. Gopalakrishnan, Mater. Res. Bull. **35**, 559 (2000).

[17] T. Horikubi, T. Mori, H. Nonobe, and N. Kamegashira, J. Alloys Compd. **289**, 42 (1999).

[18] B.C. Tofield and W.R. Scott, J. Solid State Chem. **10**, 183 (1974).

[19] J.F. Mitchell, D.N. Argyriou, C.D. Potter, D.G. Hinks, J.D. Jorgensen, and S.D. Bader, Phys. Rev. B **54**, 6172 (1996).

[20] N. Kamegashira, T. Mori, A. Inamura, and Y. Hinatsu, J. Alloys Compd. **302**, L6 (2000).

[21] M. Fang, M. Kato, K. Yoshimura, and K. Kosuge, J. Alloys Compd. **317-318**, 136 (2001).

[22] Z. Serpil Gönen, J. Gopalakrishnan, and B.W. Eichorn, Solid State Sci. **4**, 773 (2002).

[23] T. Horikubi and N. Kamegashira, Mater. Chem. Phys. **65**, 316 (2000).

[24] R.J. Bouchard, J.F. Weiher, and J.L. Gillson, J. Solid State Chem. **21**, 135 (1977).

[25] J.B. Goodenough, in *Magnetism in Metals and Metallic Compounds*, edited by J. T. Lopuszanski, A. Pekalski, and J. Przystawa (Plenum, New York, 1976), p. 52.

[26] J.B. Goodenough, A. Wold, R.J. Arnott, and N. Menyuk, Phys. Rev. **124**, 373 (1961).

[27] J.-S. Zhou, H.Q. Yin, and J.B. Goodenough, Phys. Rev. B **63**, 184423 (2001).

[28] J.B. Goodenough, R.I. Dass, and J.-S. Zhou, Solid State Sci. **4**, 297 (2002).

[29] W.H. Meiklejohn and C.P. Bean, Phys. Rev. **102**, 1413 (1956); **105**, 904 (1957).

[30] J.-S. Zhou and J.B. Goodenough, Phys. Rev. B **68**, 054403 (2003).

[31] T. Kimura, S. Ishihara, H. Shintani, T. Arima, K.T. Takahashi, K. Ishizaka, and Y. Tokura, cond-mat/0211568 (unpublished).